Structural Characterization of Oriented Polyacetylene Films Grown by the Liquid Crystal Method

N. Coustel, N. Foxonet, J. L. Ribet, and P. Bernier

Groupe de Dynamique des Phases Condensées, Université des Sciences et Techniques du Languedoc, Pl. E. Bataillon, 34095 Montpellier Cedex 05, France

J. E. Fischer*

Laboratory for Research on the Structure of Matter, University of Pennsylvania, 3231 Walnut Street, Philadelphia, Pennsylvania 19104-6272

Received March 19, 1991; Revised Manuscript Received June 20, 1991

ABSTRACT: We present a systematic study of the morphology of polyacetylene films, intrinsically oriented during the synthesis using the nematic phase of a liquid crystal as the Ziegler–Natta catalyst solvent. Orientation of the nematic phase, and hence the polymer, was achieved by gravitational flow combined with a vertical 4.7-T magnetic field. Using scanning electron microscopy, polarized Raman and infrared spectroscopies, and four-circle X-ray diffraction, we show that these films consist of distinct well-oriented and unoriented layers, the latter becoming more important for thicker films. Aging the catalyst at a higher temperature leads to a reduction in the polymerization rate and a decrease in the nonoriented fraction. n and p doping of the best films consistently produced parallel conductivities in the range 20 000 S/cm. We propose a model based on polymerization kinetics that explains the existence of different morphologies within a single "film".

Introduction

In 1974, Shirakawa and co-workers polymerized for the first time a film of polyacetylene, $(CH)_x$. This material had a fibrillar morphology (fibril diameter 200–600 Å), a high crystallinity (up to 95%), and a density in the range 0.3–0.6 g/cm^3 (ideal value 1.16 g/cm^3) and showed semiconducting properties in the neutral state and metallic behavior upon doping.[1] Transmission electron microscopy and X-ray and electron diffraction established that the $(CH)_x$ chains were oriented along the fibrils, while the fibrils themselves were randomly oriented. Several techniques were then developed to induce a *macroscopic* orientation of the film and consequently of the chains: film stretching,[1] shearing of the catalyst mixture during the polymerization,[2] and pseudoepitaxial synthesis.[3] The best mosaic was obtained by stretching after aging of the catalyst at 150–200 °C.[4,5] Aging at higher temperatures was found to decrease the polymerization rate and to improve the mechanical properties of films, thus allowing greater draw ratios before fracture. Nevertheless, stretching can induce defects and breaks of the fibrils, which limit the conductivity. It is then interesting to develop techniques that induce a significant orientation of the chains but do not require mechanical treatment of the film after polymerization.

Araya et al.[6] developed a polymerization technique using an ordered molecular matrix consisting of a nematic liquid crystal (LC) as the *solvent* for the usual Ziegler–Natta catalyst. Orientation of the $(CH)_x$ fibrils occurs during the polymerization and is determined by the orientation of the LC molecules. A quiescent nematic phase consists of random domains of oriented molecules. Therefore, with no external influence, the LC induces only microscopically oriented domains for the fibrils.[7] If the LC is macroscopically oriented by gravitational flow, the polymerization of well-oriented fibrils is encouraged.[6] Akagi et al.[8] produced similarly oriented films using the horizontal magnetic field effect on the LC molecules.

We combined the gravitational flow and magnetic field methods to enhance the nematic order in an effort to improve the orientation[9] and also studied the effect of polymerization kinetics by varying the catalyst aging temperatures from 35 to 75 °C.[10] The slower kinetics after 75 °C aging produced films with better morphology. Surprisingly, we found from polarized infrared absorption spectra that the apparent degree of orientation decreases with increasing film thickness, suggesting the presence of some previously unknown morphological phenomena during film growth. Therefore, we conducted a systematic study of morphology and preferred orientation versus thickness and growth rate using scanning electron microscopy (SEM), polarized Raman and infrared (IR) spectroscopies, and four-circle X-ray diffraction (XRD). In addition to providing more information on the liquid crystal method, these experiments were designed to fully characterize the film morphology before studying the structural and conducting properties upon doping of these films.

Experimental Section

Oriented polyacetylene films were prepared by using the Araya method.[6] A standard $Ti(OBu)_4$–$Al(Et)_3$ catalyst was used with [Ti] = 0.05 mol/L and a ratio [Al]/[Ti] = 2. The catalyst was typically aged 1 h at 35 °C; a few experiments were done with 75 °C aging. The solvent consisted of an equimolar mixture of the two liquid crystals 4-(*trans*-4-*n*-propylcyclohexyl)ethoxybenzene and 4-(*trans*-4-*n*-propylcyclohexyl)butoxybenzene supplied by E. Merck. The initial pressure of the C_2H_2 monomer was in the range 400–760 mmHg. We ordered the LC matrix with a magnetic field alone (called HMF, horizontal magnetic field, hereafter) or from the combination of a magnetic field and gravitational flow (called VMF, vertical magnetic field, hereafter). Preliminary data on the orientation of the $(CH)_x$ films have been published elsewhere.[9] The HMF synthesis is similar to the Akagi method.[8] The polymerization temperature is fixed between 10 and 13 °C in order to maintain the nematic phase. The reaction flask is placed in a container filled with water (both were between the magnet poles), which was connected to a regulated temperature unit. We used a 2-T horizontal magnetic field. In the VMF method (4.7 T), we cooled the catalyst mixture to about 10 °C just before its introduction into the magnet, but the temperature probably increased during the polymerization because the reaction flask was not thermostated. We observed that the thickness t depends on the polymerization time; 5 min gave $t < 3$ μm, and $^1/_2$–1 h gave $10 < t < 20$ μm.

The characterization techniques used in this work probe different aspects of film morphology and preferred orientation.

0024-9297/91/2224-5867$02.50/0

SEM gives the surface topography and Raman backscattering probes only the outermost 1000 Å approximately. In contrast, IR spectroscopy and XRD were done in transmission, so both methods give properties averaged over the film thickness. The degree of preferred orientation is deduced from polarized IR by recording the absorbance anisotropy ratio (R) of the vibrational modes at 745 and 1015 cm^{-1} for cis and trans isomers, respectively. These intrachain modes are independent of interchain correlations and thus do not distinguish between amorphous and crystalline phases. Their intensities vanish for polarization parallel to the chain; thus, the degree of preferred orientation is given by $\theta(R) = \cos^{-1}[2R - 1/2R + 1]^{1/2}$ where $R = A_\perp/A_\parallel$.[11] Here θ denotes the average chain orientation with respect to the principal orientation axis of the film, as established by the LC orientation. Note that R is derived from only two data points obtained with orthogonal polarizations; this means that (a) the technique gives no information about the actual distribution of chain axes and (b) the presence of some amorphous or crystalline unoriented material (for which $R = 1$ and thus $\theta = 55°$) would cause θ for the oriented portion to be overestimated. Also, in what follows we quote 2θ values for comparison with the mosaic full width at half-maximum (fwhm) derived from XRD.

We used a horizontal four-circle X-ray diffractometer to measure the detailed distribution of chain axes, the correlation lengths parallel and perpendicular to the chains, and the fraction of unoriented material. Three different scans were performed on each sample, equivalent to three trajectories on a Debye–Scherrer fiber diagram: radial Q scans along the average ($hk0$) and ($00l$) directions at fixed χ ("equatorial" and "meridional", respectively), and χ scans at fixed Q ("azimuthal" at fixed radius). By definition $\chi = 0°$ corresponds to the ($hk0$) axis (we assume that the h and k directions are completely averaged out). A comparison of Q scans in the region of the intense (020)/(110) doublet with $\chi = 0°$ and $\chi = 90°$ is thus geometrically equivalent to the polarized IR experiment, while a χ scan at the maximum Q of the doublet can be analyzed in terms of a Gaussian peak plus a constant, representing respectively, the diffraction from oriented chains and that from unoriented material plus background (the latter two can be separetly identified from the Q scan at $\chi = 90°$ since we did not observe any measurable Q-dependent diffuse scattering associated with amorphous material). We assumed that the "unoriented" crystallites were completely random. Radial peaks were fitted with Gaussian line shapes. The best fits to the χ scans were obtained with mixed Gaussian plus Lorentzian functions, although in what follows we will quote only the fwhm's from the purely Gaussian fits for simplicity.

We used a 1.5-kW copper-sealed-tube, vertically focusing graphite (004) monochromator and Soller slit after the sample. All measurements were done in transmission through a 6-mm aperture. The Q and χ resolutions were approximately 0.02 $Å^{-1}$ and 3.3° fhwm, respectively. In order to obtain sufficient scattering volume from these very thin films, X-ray samples were made by carefully folding the as-grown material into 50–100 μm-thick assemblies. We verified that this procedure did not affect the measured mosaic fwhm's by measuring one mosaic distribution before folding. The assemblies were thermally isomerized for $^1/_2$ h at 160 °C under dynamic vacuum to avoid confusion between cis and trans Bragg reflections. The O-ring-sealed sample holder was fitted with thin Ni windows and loaded in an argon-purged glovebox.

Results

The typical procedure in all the polymerization experiments was to leave the reaction vessel in the magnetic field until the desired thickness was obtained. We were initially concerned about the lack of a thermostat in the VMS method, so we performed two preliminary runs to test the consequences of possible temperature variations during polymerization. These consisted of polymerizing in the magnet until a transparent film was obtained (500–1000 Å thick) and then continuing the growth for up to 2 h outside the magnet (during which time the LC temperature surely increased above the nematic transition).

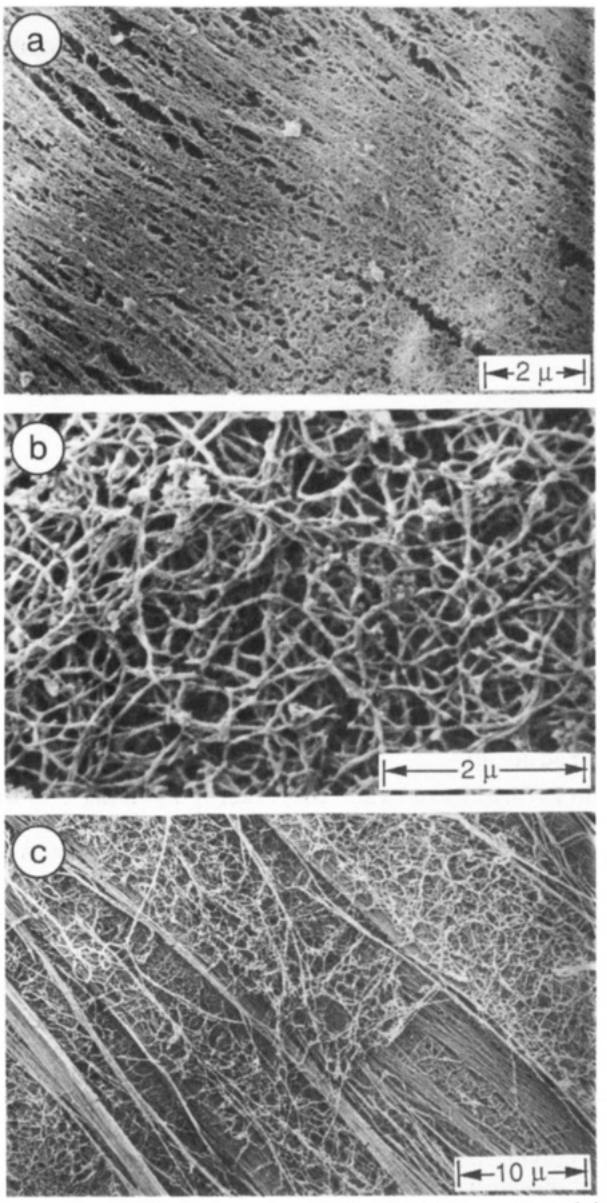

Figure 1. SEM photos of a thick $(CH)_x$ film oriented by polymerizing on a liquid crystal substrate. The nematic phase is aligned in a horizontal magnetic field: (a) surface that was in contact with the glass reactor wall; (b) free surface exposed to the gas monomer; (c) interface exposed by peeling apart the two distinct layers making up the film.

This nonstandard procedure yielded well-oriented opaque films 1–2 μm thick, which shows that the oriented LC phase, initially established by the VMF, is maintained by the growth of the first oriented fibrils. In other words, a macroscopic orientation of LC molecules persists throughout the polymerization even if the reaction temperature increases above the nematic phase transition. This result is also significant because it proves that the existence of nonoriented material under some growth conditions (discussed below) is not attributable to the lack of temperature control in the VMF method but is rather an intrinsic feature of the polymerization.

(a) Scanning Electron Microscopy. Figure 1 shows typical SEM photos of the surface topography resulting from HMF film growth (approximately 10 μm thick). The surface of the glass reactor side (Figure 1a) shows a mat of partially oriented fibrils; this surface is fairly specular in reflected light. The opposite surface on the gas side (Figure 1b) shows random fibrils reminiscent of unstretched Shirakawa material. This surface appears dull

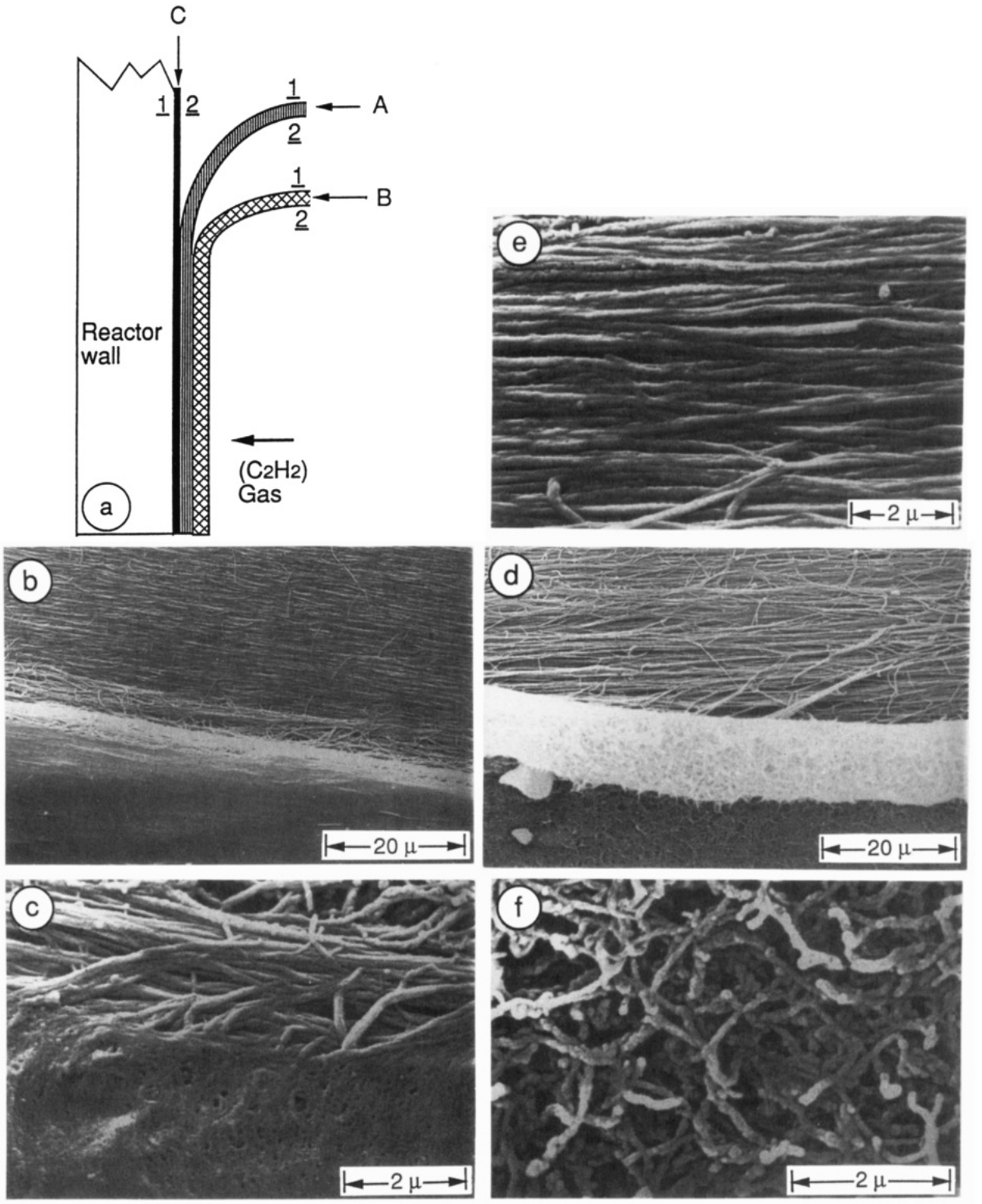

Figure 2. Similar to Figure 1, but with the combined alignment effect of gravitational flow and vertical magnetic field. (a) Schematic representation of three distinct layers, which can be peeled apart: layer A, oriented fibrils; layer B, unoriented fibrils; layer C, dense skin of poorly oriented fibrils. The surfaces 1 and 2 of each layer denote, respectively, the side closest to and farthest from the reactor wall. (b) Surfaces A-1 (top) and C-1 (bottom); the bright central band (overexposed) is the interface between C-2 and A-1, shown with a higher magnification in c. (d) Surfaces A-2 (top, magnified in e) and B-2 (bottom, magnified in f); the central band is the surface B-1.

to the eye. There is a rather abrupt transition between oriented and unoriented material. In fact the two regions can be peeled apart into two distinct layers, which reveals the surface of a well-oriented layer within the film (Figure 1c), on which a small amount of unoriented material remains. The fibril diameter is in the range 100–200 Å throughout the entire film thickness.

Thick VMF films ($t > 3$ μm) can be peeled apart into three distinct layers. This is shown schematically in Figure 2a along with a labeling scheme to help understand the SEM photos. For reasons that will become clear later, the intermediate layer is denoted A, while the outermost layer and the one in contact with the glass are denoted B and C, respectively. For each layer, the surfaces 1 and 2 are

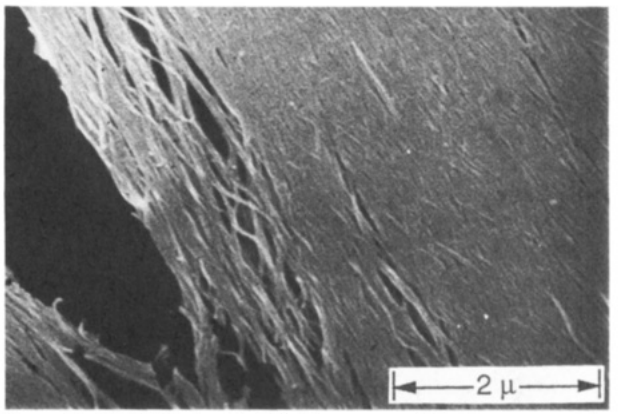

Figure 3. SEM photo of a thin film prepared by the same method as the film shown in Figure 2. This film cannot be peeled apart, and the photo is representative of both sides.

closest to, and farthest from, the glass, respectively. Before peeling, C-2 is in contact with A-1, etc.

Figure 2b was taken near the torn edge of a thick VMF film after peeling half a sample. The bottom of the photo is the nonpeeled C-1 surface, which appears as a dense and shiny featureless skin with no apparent fibrillar morphology, as is found in $(CH)_x$ film prepared by the Durham/Graz precursor method.[12] The top of the photo (peeled part of the sample) shows well-oriented fibrils comprising layer A. The bright band between these regions is the (overexposed) "interface" between C-2 and A-1, which is shown with a higher magnification in Figure 2c. This shows that most of the dense skin C is formed of poorly oriented fibrils. Figure 2d was taken after peeling layer B away from layer A. The bottom of this photo is B-2 (the dull surface in contact with the gas monomer), and the bright band is the exposed surface B-1. This photo shows that layer B consists entirely of unoriented fibrils with apparently a very low density. The upper part of Figure 2d is the surface A-2; along with Figure 2b, this shows that layer A consists entirely of well-oriented material. Parts e and f of Figure 2 show the upper and lower portions of Figure 2d with a higher magnification. The apparent fibril diameter ~1000 Å is probably exaggerated in these photos by an excessively thick gold overcoating. The measured density of these thick films is close to the density of the unoriented material.

Thinner VMF films ($t < 3$ μm) do not exhibit this multilayer morphology. Figure 3 shows such a film that cannot be peeled and that shows dense oriented fibrils (well detected at the torn edge) on both surfaces. The density of thin films is close to the ideal density, consistent with the absence of low-density unoriented fibrils.

(b) Infrared Absorption. Figure 4 shows polarized IR spectra for "thick" and "thin" films obtained by the VMF method. Both films show comparable intensities for the cis and trans modes at 745 and 1015 cm^{-1}, respectively. For an 8 μm film produced after aging the catalyst 1 h at 35 °C (Figure 4a), the polarization anisotropy is rather weak and we deduce $R = 1.6–1.8$; hence, $2\theta = 86°$ and 82° for the cis and trans components, respectively. Thinner films produced by exactly the same method give smaller 2θ values. In Figure 4b we show the effect of decreasing the film thickness. For $t = 1$ μm, the anisotropy is enhanced, and we find $2\theta = 36°$ and 32° for cis and trans, respectively. Interference fringes are clearly observed in the parallel spectrum. Increasing the aging temperature to 75 °C enhances the anisotropy only slightly; 2θ is somewhat lower with this latter method if we compare two samples with similar thicknesses. These and similar

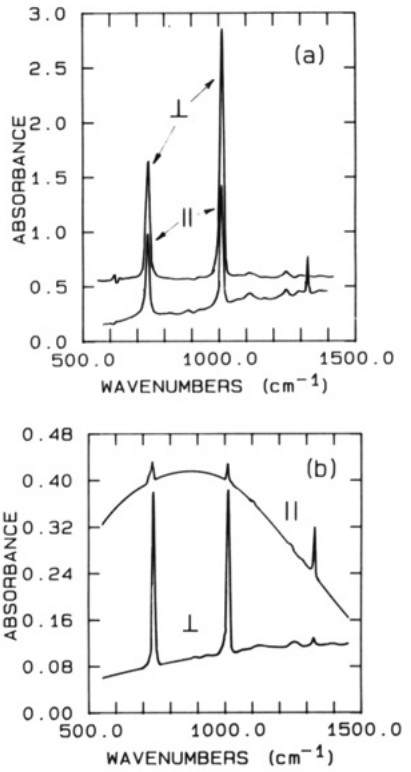

Figure 4. Typical polarized IR absorption spectra for "thick" and "thin" films of polyacetylene (approximately a 60:40 ratio of cis and trans isomers). The degree of preferred orientation is obtained from the absorbance anisotropy of the vibrational modes at 745 and 1015 cm^{-1} for cis and trans isomers, respectively. (a) Data for a film 8 μm thick, catalyst aged 1 h at 35 °C; top and bottom spectra correspond to polariztion perpendicular and parallel to the average chain axis, respectively. The top curve has been displaced upward by 0.5 units for clarity. (b) Data for a similar film 1 μm thick (top = parallel, bottom = perpendicular). The weaker anisotropy of the thick film is evidence for a reduced degree of preferred orientation.

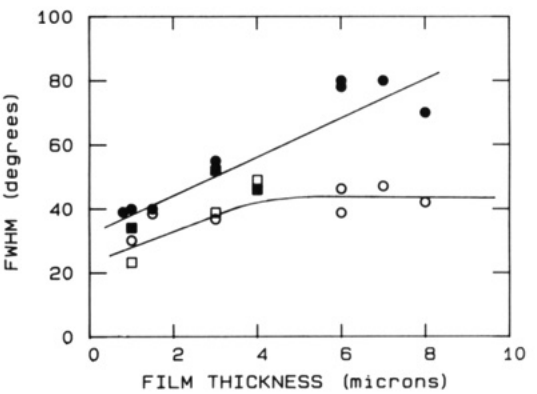

Figure 5. Thickness dependence of the chain axis mosaic distributions, as determined from IR absorption anisotropy (filled symbols) and XRD (open symbols). Circles and squares denote films prepared after catalyst aging at 35 and 75 °C, respectively.

IR results are collected in Figure 5 as the solid symbols: circles for 35 °C aging and squares for 75 °C aging. These are averages of the cis and trans values. In general, 2θ increases roughly linearly with thickness.

(c) X-ray Results. Figure 6 shows XRD profiles for "thin" and "thick" films obtained with 75 and 35 °C catalyst aging temperatures, respectively. Open and filled squares are the measured points while the solid curves are least-squares fits as described below. The top panels show superpositions of radial Q scans along the two principal azimuths. For both films we observe the intense (020)/(110) doublet centered at 1.75 $Å^{-1}$ with $\chi = 0°$. With χ

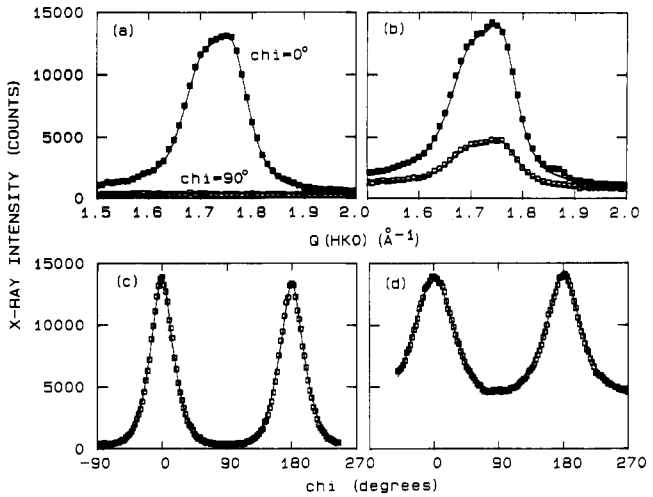

Figure 6. Typical XRD results for thin and thick films. In a and b are shown radial scans at two azimuths corresponding to equatorial, or ($hk0$) orientations (χ = 0°, filled squares), and meridional, or ($00l$) orientations (χ = 90°, open squares). Solid lines are fits to the data based on Gaussian profiles for the (020) and (110) reflections of the *trans*-$(CH)_x$ structure. The presence of a substantial ($hk0$) intensity on the ($00l$) azimuth in Figure 6b signals the existence of a large nonoriented fraction in this film. In c and d are shown χ azimuthal scans at fixed Q = 1.75 Å^{-1}. For the thin film, the ($hk0$) intensity falls to background at $\chi = \pm 90°$, consistent with the absence of nonoriented material. Squares indicate data; solid curves are fits to Gaussian profiles plus a constant background.

= 90° the thin film (Figure 6a) exhibits only a featureless background while the thick one (Figure 6b) still exhibits substantial ($hk0$) intensity. This indicates the absence of random crystallites in the former but a significant amount of unoriented material in the latter. The ratio [intensity (90°)/intensity (0°)] is taken as a measure of the nonoriented fraction. The bottom panels show χ scans at fixed Q = 1.75 Å^{-1}. The thin film (Figure 6c) exhibits fairly sharp peaks at 0° and 180°, with the signal falling to background in between. In contrast, the thick film (Figure 6d) exhibits broader peaks and substantial ($hk0$) scattering above background at χ = 90°, corresponding to an ($00l$) azimuth. The overall χ dependence is adequately represented by peaks on the equator plus a constant (solid curve), indicating that the ($hk0$) scattering that appears on the ($00l$) azimuth is a signature of a completely random crystalline material.

The fitted Gaussian fwhm values from the χ scans are added to the IR-derived data in Figure 5 as the open symbols. Again, we note an increasing fwhm with increasing thickness, although less dramatic for the XRD data as compared to the IR values. In fact, the XRD-derived fwhm shows a tendency to saturate at the higher thicknesses, while the IR-derived values continue to increase with increasing thickness. Aside from one film with t = 4 μm, the IR values are systematically greater than the XRD ones; the discrepancy is most pronounced for the thickest films.

Figure 7 shows the thickness dependence of the nonoriented fraction derived from the fits to the radial scans (top, Figure 6). With 35 °C aging the nonoriented fraction increases linearly with thickness, reaching 40–60% at 8 μm. With 75 °C aging, only at 4 μm is there a detectable nonoriented fraction.

The best conditions for aging the catalyst appear to be 3 h at 75 °C. Longer aging (17 h) results in a decrease in the overall crystallinity, as evidence by the appearance of a diffuse peak on the low-Q side of the (020)/(110) doublet. The best mosaic we obtained, 23° fwhm, is comparable to

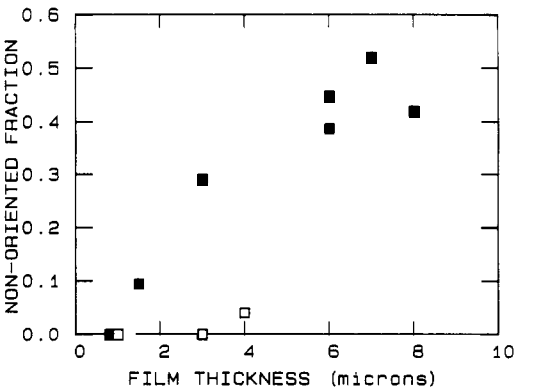

Figure 7. Nonoriented fraction versus film thickness. Open and filled squares denote 35 and 75 °C catalyst aging, respectively.

some stretch-oriented values[4] but considerably worse than others.[5] We found no significant variation of the radial line width with the preparation conditions, thickness, or (for thick films) azimuth, suggesting that the crystallite size is intrinsic to the fibrils and independent of the degree of alignment.

Discussion

In order to perform reliable physical measurements on oriented $(CH)_x$, it is essential to characterize correctly the orientation of the chains and the fibrils, on the microscopic and macroscopic scales. Of particular importance for the interpretation of transport measurements is the question of the homogeneity of the orientation throughout the thickness of the film. Previous IR investigation of Akagi samples[8,11] showed a full angle of the orientation dispersion 2θ = 52–56°, while direct observation of SEM pictures obtained by many authors imply $2\theta \cong$ 5–10°.[6,8,11] Our present SEM results show that thin and thick films present different morphologies and that the degree of preferred orientation at the surfaces (Figure 1a,b) does not reflect systematically the orientation in the bulk (Figure 1c). Thin films have well-oriented fibrils on both faces and appear dense (Figure 3), while thick films present three distinct zones. Close to the glass reactor, there is the dense skin of poorly oriented fibrils (Figure 2b,c), and on the opposite face, there is a low-density layer of nonoriented fibrils (Figure 2d,f) (on the side where the monomer gas arrives). Between these two layers, well-oriented fibrils appear (Figure 2b,d,e). The existence of these three zones is consistent with most experimental results; polarized Raman confirms the degree of surface orientation while the apparent discrepancy between IR and XRD results (2θ versus fwhm) on films thicker than 3–4 μm exists because the determination of the orientation from intrachain modes using $A_\perp/A_\parallel$ mixes the effects of finite mosaic and unoriented chains (Figure 5). The four-circle XRD data allow a separate determination of the in-plane mosaic and nonoriented fraction. This fraction grows linearly with film thickness (Figure 7). For films above 4 μm we conclude that the finite mosaic does not change but the unoriented fraction increases and consequently 2θ increases.

These different morphologies within a single film exist because the polymerization of acetylene depends on the gas monomer and catalyst diffusion processes inside the catalytic medium. These kinetic effects control the polymerization rate and, thus, the density, the thickness,[13] and the degree of preferred orientation. In a previous work concerning the nonoriented polyacetylene, Aldissi[13] described the polymerization process (deduced from observations) as follows. First, there is a rapid consumption of acetylene corresponding to the rate of initiation at

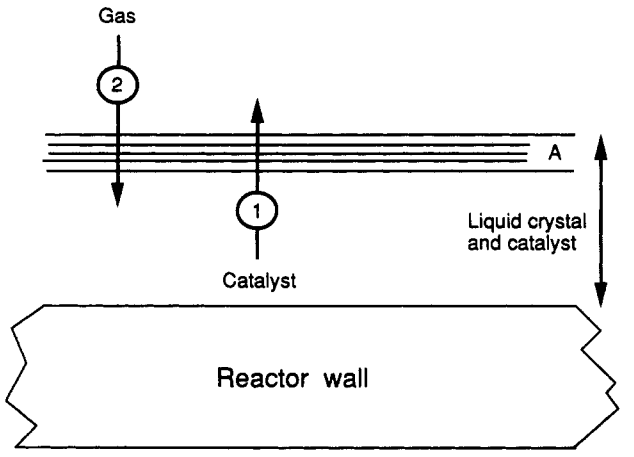

Figure 8. Schematic representation of gas and catalyst counterdiffusion through layer A, the basis of a kinetic model (discussed in the text), which explains the trilayer morphology described in Figure 2.

the surface of the solution. Next, this first-grown film retards further polymerization because of the limited diffusion of the acetylene monomer through the film and the limited diffusion of the catalyst to the surface of the film in contact with acetylene. These diffusion processes become the rate-determining steps for further polymerization. If the first layer of fibrils corresponding to the first part of polymerization is too dense, the polymerization is rapidly inhibited.

In our case the polymerization process is similar; differences are due to the solvent, which is a liquid crystal instead of toluene. Consequently, we speculate that these different steps lead to the existence of layers of fibrils, which show different densities and degrees of preferred orientation. During the initiation of the polymerization, oriented fibrils can grow into the LC (layer A, Figures 2a and 8). The thickness of this layer is limited to $\cong 3$ μm for the usual 35 °C aging of the catalyst, while larger values can be obtained if the aging temperature is 75 °C. Further polymerization produces a rather unoriented material on both sides of layer A due to the counterdiffusion of C_2H_2 and the catalyst through layer A. Growth of layer B (Figure 2a) depends on the catalyst diffusion through layer A (arrow 1, Figure 8). The preferred orientation is lost because the restricted volume accessible to the diffusing LC molecules hinders the effect of the magnetic field;[14] the diffusing LC molecules need a finite volume of the nematic phase to be oriented. The poor orientation of the fibrils in the dense layer C (Figure 2a) is related to the diffusion of C_2H_2 near the reactor wall (arrow 2, Figure 8). Fibrils grow against the glass, and the limited degree of freedom involves formation of a dense and shiny film. This effect was previously noticed during the polymerization of the nonoriented material when the catalyst mixture flowed along the vessel wall.[1] The corresponding layer appears less dense in the case of the HMF synthesis, which occurs in a quiescent catalytic medium. A similar effect is observed with unoriented $(CH)_x$ synthesis.[13] Flowing the catalyst medium along the reactor wall leads to fibril growth in a limited volume of solvent. This means that, beyond a given thickness, the fibrils in contact with the glass will spread out and further growth becomes two-dimensional. This effect produces the dense skin. By polymerizing in a quiescent, hence larger, volume of catalyst solution, fibrils continue to grow far from the flask wall; growth now occurs in three dimensions, and no dense skin is observed. But, we observe that the fibrils of layer C are poorly oriented, so the support effect still annihilates the field-induced orientation of the LC molecules. This model explains why thick films cannot be obtained with homogeneous orientation throughout the entire thickness.

We know that polymerization kinetics mainly depend on the catalyst activity. Previous results[13] on the synthesis of nonoriented $(CH)_x$ show that the polymerization rate changes with catalyst concentration, which in turn affects the density and film thickness. Aldissi[13] proved that a high concentration of catalyst (solvent is evaporated from the catalytic medium) rapidly produces a very dense first layer. In our experiment, we observe that the polymerization rate affects fibril orientation. By modifying the aging of the catalyst from 35 to 75 °C, we have decreased the polymerization rate,[10] as measured by the film thickness versus the polymerization time. Analysis of the preferred orientation with IR and XRD shows that the best values are obtained for thin films with aging at 75 °C (Figure 5), with good agreement between IR and XRD up to 4 μm. This means that the oriented layer A continues to grow for $t > 3$ μm. Aging at 75 °C also produces lower nonoriented fraction values compared to 35 °C aging for a similar thickness (Figure 7); unoriented material is undetectable below 3 μm.

Consequently to these morphology observations and comparisons between the polymerization of nonoriented and oriented $(CH)_x$, we make some speculations about the influence of the diffusion rate of the gas and the catalyst on the fibril orientation. A lower polymerization rate implies a decrease of layer A density; thus, process 2 (arrow 2, Figure 8) is less limited. Thus, fibril growth in contact with oriented LC continues longer as compared to aging at 35 °C. The density of layer A controls process 2 but not process 1 (arrow 1, Figure 8) because only the nonoriented layer B is growing above a certain thickness (Figure 7). We suggest that the catalyst diffusion is enhanced by the capillarity along the fibrils to be in contact with the gas. By aging the catalyst at 75 °C, layer B appears only above a thickness of 3 μm (Figure 7). This means that, if process 2 is not limited, process 1 does not affect the morphology of the film. We propose that (i) the diffusion rate of the gas monomer mainly controls the polymerization up to a critical thickness, (ii) the density of layer A affects the diffusion of the gas but not of the catalyst, and (iii) above a critical thickness, the polymerization into the LC is inhibited and only a nonoriented layer is still growing due to the catalyst diffusion.

The multilayer morphology accounts for the increase in the nonoriented fraction with an increase in the total thickness. Figure 5 suggests an additional thickness dependence of the fwhm within the well-oriented layer. This could be due either to an increasing dispersion in the fibril orientation with increasing t or to a degradation of the mosaic inside a single fibril with increasing polymerization time (see below).

Shirakawa et al.[11] give an empirical relation between the orientation angle and a virtual stretching ratio (l/l_0). Applying this relation to our best mosaic values, we find, respectively, $l/l_0 = 3.5$–4 and $l/l_0 = 6$ for aging at 35 and 75 °C.[11] So, if we avoid unoriented fraction formation by aging the catalyst at 75 °C, the mosaic fwhm approaches the values obtained by some stretching methods.[4] Kinetic phenomena are apparently important in stretch-oriented films as well. New techniques[5] involve aging of the catalyst to improve the stretching properties and give $l/l_0 = 10$–15 similar to the Graz–Durham films.[12] Tsukamoto,[5] after aging the catalyst, decreases the polymerization rate further by diluting C_2H_2 with argon (5%). This synthesis takes several hours to obtain a 5 μm film.

It is now apparent that various degrees of macroscopic and microscopic preferred orientation can be obtained by mechanical stretching, LC "pseudoepitaxy", or thermolysis of a stretch-aligned precursor. The first two methods produce fibrillar morphologies, and only for the most recent versions of stretch-aligning does one obtain consistency between macroscopic (fibril alignment via SEM, micron length scale) and microscopic (crystal alignment via XRD, 100-Å scale) orientations. This implies that the microscopic orientation is ultimately limited by the morphology within an individual fibril. Our LC results present an extreme example of this discrepancy; despite an apparent dispersion of fibril axes on the order of a few degrees (cf. Figure 2e), the best XRD-derived fwhm is 23°. Further progess in developing the stretch-alignment and LC processes would benefit greatly from diffraction experiments capable of probing the orientation within a single fibril.

Measurements of the electrical conductivity parallel to the chains are quite consistent with the morphological results presented here. Foxonet et al.[10] showed that the conductivity of doped films drops systematically with increasing thickness; this can be attributed to unoriented layer formation. The parallel conductivity of thin films dope with I_2 vapor is between 20 000 and 40 000 S/cm.[9,10] Upon electrochemical doping with potassium, similar thin films give a maximum parallel conductivity of 17 500 S/cm.[15] We note that n and p doping give similar values. Using this second method to dope a nonoriented sample with potassium, Schacklette and Toth[16] and Fite[17] found 450 S/cm. If we report both values on the phenomenological law $\sigma_\parallel = \sigma_0(l/l_0)^2$,[18] we find $l/l_0 = 6$ ($\sigma_\parallel$ is the conductivity parallel to the chain axis and σ_0 is the conductivity of an unoriented sample). This value corresponds to the one deduced from the orientation angle. Thus, we propose that the conductivity improvement is mainly due to an orientation effect of the fibrils. While our conductivity values are considerably below some values obtained with recent stretched films (σ = 100 000 S/cm), they are quite reproducible.

Conclusion

In this work, we used the Araya method to prepare oriented films of polyacetylene. Fibrils were intrinsically aligned during polymerization by a liquid crystal matrix. We combined the gravitational flow and magnetic field methods to improve the orientation of the fibrils. We used four complementary techniques to analyze the morphology of the films: SEM, polarized Raman and infrared spectroscopies, and four-circle X-ray diffraction, the first two giving the surface orientation while the last two provide properties averaged over the film thickness. The discrepancy between IR and XRD measurements confirms that these films consist of well-oriented and nonoriented layers (consistent with SEM), with the latter becoming more important for thicker films. By aging the catalyst at a higher temperature, we reduced the polymerization rate and observed a decrease in the nonoriented fraction. The best XRD-derived fwhm of 23° was obtained for thin films. We are now unable to determine if the combined effect of gravitational flow and magnetic field LC alignment is better than either alone since XRD was not performed in the earlier studies and IR can give an erroneous mosaic distribution due to the nonoriented layer. We propose a model based on the polymerization kinetics that explains the existence of different morphologies within a single film. A film 1 μm thick has been used to carefully follow the evolution of the parallel electronic conductivity upon electrochemical doping with potassium. Results are reproducible, and the conductivity behavior has been correlated with the structural evolution of the system.[14] Conductivity experiments versus the doping level of potassium and the temperature are in progress. The fact that the parallel conductivity of our doped films is more reproducible than the values obtained from stretch-aligned films suggests the possibility of uncontrollable defects introduced during stretching.

Acknowledgment. We acknowledge J. L. Sauvajol for Raman studies and A. Montaner and M. Galtier for infrared spectra. P. A. Heiney provided valuable assistance during the early stages of the XRD experiments. This work was supported in part by DOE Grant DE-FCO2-86 ER 45254. The Montpellier–Pennsylvania collaboration is supported by NATO Grant 0866/87.

References and Notes

(1) Shirakawa, H.; Ikeda, S. *Synth. Met.* **1979/80**, *1*, 175.
(2) Meyer, W. H. *Synth. Met.* **1981**, *4*, 81.
(3) Yamashita, Y.; Shimamura, K.; Kasahara, H.; Monobe, K. *Synth. Met.* **1987**, *17*, 252.
(4) Lugli, G.; Pedretti, U.; Perego, G. *J. Polym. Sci., Polym. Lett. Ed.* **1985**, *213*, 129; *Mol. Cryst. Liq. Cryst.* **1985**, *118*, 43. Naarman, H.; Theophilou, N. *Synth. Met.* **1987**, *22*, 1. Akagi, K.; Suezaki, M.; Shirakwa, H.; Kyotani, H.; Shimomura, M.; Tanabe, Y. *Synth. Met.* **1989**, *28*, D1.
(5) Tsukamoto, J.; Takahashi, A.; Kawasaki, K. *Jpn. J. Appl. Phys.* **1990**, *29*, 125. Cao, Y.; Smith, P.; Heeger, A. *J. Polym. J.*, in press.
(6) Araya, K.; Mukoh, A.; Narahara, T.; Shirakawa, H. *Chem. Lett.* **1984**, 1141. Araya, K.; Mukoh, A.; Narahara, T.; Akagi, K.; Shirakawa, H. *Synth. Met.* **1987**, *17*, 247.
(7) Shirakawa, H.; Akagi, K.; Katayama, S. *J. Macromol. Sci., Chem.* **1988**, *A25* (5–7), 643.
(8) Akagi, K.; Katayama, S.; Shirakawa, H.; Araya, K.; Mukoh, A.; Narahara, T. *Synth. Met.* **1987**, *17*, 241.
(9) Rolland, M.; Ribet, J. L.; Montaner, A.; Galtier, M.; Lakhliai, Z.; Sauvajol, J. L.; Brunet, M.; Almairac, R.; Bernier, P. *Polym. J.* **1988**, *29*, 1101; *Synth. Met.* **1988**, *24*, 1.
(10) Foxonet, N.; Coustel, N.; Ribet, J. L.; Galtier, M. *Synth. Met.*, in press.
(11) Shirakawa, H.; Akagi, K.; Katayama, S.; Ito, M.; Araya, K. *International Union of Pure and Applied Chemistry Macro 88*, Kyoto Congress, Aug 1–6, 1988.
(12) Leising, G. *Polym. Commun.* **1984**, *25*, 201; *Polym. Bull.* **1984**, *11*, 401.
(13) Aldissi, M. *Polym. J.* **1982**, *23*, 246.
(14) De Gennes, P.-G. *The Physics of Liquid Crystals*; Clarendon Press: Oxford, 1974.
(15) Coustel, N.; Bernier, P.; Fischer, J. E. *Phys. Rev.* **1991**, *B43*, 3147.
(16) Shacklette, L. W.; Toth, J. E. *Phys. Rev.* **1985**, *B32*, 5892.
(17) Bernier, P.; Fite, C.; El Khodary, A. In *Chemical Physics of Intercalation*; NATO Advanced Study Institute Series 172, Legrand, A. P., Flandrois, S., Eds.; Plenum: NY, 1987; pp 271–289.
(18) MacDiarmid, A. G.; Heeger, A. J. In *Molecular Metals*; Hatfield, W. E., Ed.; Plenum: New York, 1979; p 161.

Registry No. C_2H_2, 25067-58-7; 4-(*trans*-4-*n*-propylcyclohexyl)ethoxybenzene, 80944-44-1; 4-(*trans*-4-*n*-propylcyclohexyl)-butoxybenzene, 79709-84-5.